

Enhancement of Deformation Sub-Model in an Orthotropic Material Model

Loukham Shyamsunder, Bilal Khaled and Subramaniam D. Rajan

School of Sustainable Engineering and the Built Environment, Arizona State University, Tempe, AZ

Kelly S. Carney and Paul DuBois

George Mason University, Fairfax, VA

Gunther Blankenhorn

LSTC, Livermore, CA

Abstract

A generalized tabulated three-dimensional orthotropic material model currently available in the dev version of LS-DYNA[®] as MAT_213 is enhanced with new features. MAT_213 has a modular constitutive model architecture consisting of deformation, damage and failure sub-models. The deformation sub-model has been enhanced with visco-elastic-plastic formulation with rate and temperature dependencies as well as strain-smoothing techniques to improve the stability of the analysis. Verification tests are carried out with experimentally obtained stress-strain curves at quasi-static and at higher rates of loading for the T800-F3900 unidirectional composite. Validation tests are carried out using data from high-speed projectile impacts on stacked-ply composite panels. Results show that the developed framework provides reasonable predictive capabilities.

Introduction

The need for the development of a reliable material model for composite materials led to the development of a general three-dimensional orthotropic material model [Goldberg et al., 2015]. The model is implemented as MAT_213 [Hoffarth et al., 2016] in LS-DYNA [LSTC, 2019]. The material model is modular and has three sub-models – deformation, damage and failure. The deformation sub-model is based on plasticity and is driven by a minimum of twelve tabulated stress-strain curves [Khaled et al., 2017]. Additional sets of stress-strain curves for different strain rate and temperature can be also be used. The damage sub-model predicts the reduction in the stiffness of the material. This is also driven by tabulated damage parameter input [Khaled et al., 2018]. The failure sub-model on the other hand erodes the finite element into consideration [Goldberg et al., 2015; Shyamsunder et al., 2019]. It must be noted that the use of damage and the failure sub-model is optional. The enhancements to the deformation sub-model with implementation details to predict stress relaxation is discussed in this paper. Other enhancements include automatic modification of Poisson's ratio to maintain orthotropic material property compatibility and strain rate smoothing.

Theoretical Background

The deformation model [Goldberg et al., 2015; Hoffarth et al., 2016] requires a set of twelve stress-strain curves. These are tension stress-strain curves in 1, 2 and 3 Principal Material Directions (PMD), 1, 2 and 3-direction compression, shear stress-strain curves in 1-2, 2-3 and 1-3 planes, and off-axis stress-strain curves in 1-2, 2-3 and 1-3 planes. If the composite exhibits rate and/or temperature dependency, then additional stress-strain curves corresponding to these strain rate-temperature combinations can be fed into MAT_213. A general three-dimensional constitutive law stiffness matrix formulation is used which is given by

$$\mathbf{C} = \mathbf{S}^{-1} = \begin{bmatrix} \frac{1}{E_{11}} & -\frac{\nu_{21}}{E_{22}} & -\frac{\nu_{31}}{E_{33}} & 0 & 0 & 0 \\ & \frac{1}{E_{22}} & -\frac{\nu_{32}}{E_{33}} & 0 & 0 & 0 \\ & & \frac{1}{E_{33}} & 0 & 0 & 0 \\ & & & \frac{1}{2G_{12}} & 0 & 0 \\ Sym & & & & \frac{1}{2G_{23}} & 0 \\ & & & & & \frac{1}{2G_{13}} \end{bmatrix} \quad (1)$$

The moduli are computed internally in MAT_213 using the input stress-strain curves interpolated for a given strain rate and temperature at a given point of time during the simulation. In order to avoid numerical instability due to sudden change in moduli which can be caused by a noisy strain rate, the strain rate in each PMD are smoothed using the following equation,

$$\dot{\boldsymbol{\epsilon}}_{n+1}^{avg} = (1 - FILT) \times \dot{\boldsymbol{\epsilon}}_{n+1} + FILT \times \dot{\boldsymbol{\epsilon}}_n^{avg} \quad (2)$$

where n presents the previous time step. $FILT$ is a user-specified parameter with a value between 0 and 1. MAT_213 is further enhanced to predict the behavior of a viscoelastic-viscoplastic material [Achstetter, 2019]. This requires the deformation sub-model to be described by equilibrium and viscous stress-strain components. The viscous component is considered to be rate dependent. The moduli obtained for quasi-static rate are used to construct the equilibrium stiffness matrix, \mathbf{C}_e . In the formulation of the stiffness matrices, \mathbf{C} and \mathbf{C}_e , the Poisson's ratios are modified internally in MAT_213 if orthotropic property compatibility is not satisfied [Lempriere, 1968]. The following checks and corrections are done for each time step and at every Gauss point.

Step 1: Input- ν_{21} , ν_{32} , ν_{31} , E_{11} , E_{22} , E_{33} and correction factor, $c_{prf} = 0.95$.

Step 2: If $|\nu_{21}| \geq \sqrt{\frac{E_{22}}{E_{11}}}$, go to Step 3, else go to Step 4.

Step 3: Set $\nu_{21} = c_{prf} \sqrt{\frac{E_{22}}{E_{11}}}$ and set FLAG21 = 1.

Step 4: If $|\nu_{32}| \geq \sqrt{\frac{E_{33}}{E_{22}}}$, go to Step 5, else go to Step 6.

Step 5: Set $\nu_{32} = c_{prf} \sqrt{\frac{E_{33}}{E_{22}}}$ and set FLAG32 = 1.

Step 6: If $|\nu_{31}| \geq \sqrt{\frac{E_{33}}{E_{11}}}$, go to Step 7, else go to Step 8.

Step 7: Set $\nu_{31} = c_{prf} \sqrt{\frac{E_{33}}{E_{11}}}$ and set FLAG31 = 1.

Step 8: Compute, $\det 2 = 1 - \nu_{21}^2 \frac{E_{11}}{E_{22}} - \nu_{32}^2 \frac{E_{22}}{E_{33}} - \nu_{31}^2 \frac{E_{11}}{E_{33}}$

Step 9: If $\left(\nu_{21} \nu_{32} \nu_{31} \frac{E_{11}}{E_{33}} \geq \frac{1}{2} \right)$ or $\left(\nu_{21} \nu_{32} \nu_{31} \frac{E_{11}}{E_{33}} \geq \frac{\det 2}{2} \right)$ or $\left(\frac{\det 2}{2} \geq \frac{1}{2} \right)$, go to Step 10a, else continue with stiffness matrix formulation.

Step 10a: If FLAG21 = 1 Set $\nu_{21} = c_{prf} \nu_{21}$, and go to Step 10b.

Step 10b: elseif FLAG32 = 1 Set $\nu_{32} = c_{prf} \nu_{32}$, and go to Step 10c.

Step 10c: elseif FLAG31 = 1 Set $\nu_{31} = c_{prf} \nu_{31}$, and go to Step 10d.

Step 10d: else Set $\nu_{21} = c_{prf} \nu_{21}$, $\nu_{32} = c_{prf} \nu_{32}$ and $\nu_{31} = c_{prf} \nu_{31}$, and go to Step 8.

The default value of c_{prf} is taken as 0.95 and this ensures that the correction needed to satisfy the material relationships is small. The viscous stiffness matrix is given by the following equation,

$$\mathbf{C}_v = \mathbf{C} - \mathbf{C}_e \quad (3)$$

The trial stress is given by the summation of equilibrium trial stress and the viscous trial stress,

$$\boldsymbol{\sigma}_{TRIAL} = \boldsymbol{\sigma}_{TRIAL}^e + \boldsymbol{\sigma}_{TRIAL}^v \quad (4)$$

where

$$\boldsymbol{\sigma}_{TRIAL}^e = \boldsymbol{\sigma}^e + \mathbf{C}_e \dot{\boldsymbol{\epsilon}}^{avg} \Delta t \quad (5)$$

$$\boldsymbol{\sigma}_{TRIAL}^v = \boldsymbol{\sigma}^v \circ \boldsymbol{\beta} + [\mathbf{C}_v \circ \mathbf{B}] \dot{\boldsymbol{\epsilon}}^{avg} \Delta t \quad (6)$$

In Equation (6), \circ stands for Hadamard product. $\boldsymbol{\beta}$ is the viscoelastic decay vector given by,

$$\boldsymbol{\beta} = \left[e^{-\beta_{11}\Delta t} \quad e^{-\beta_{22}\Delta t} \quad e^{-\beta_{33}\Delta t} \quad e^{-\beta_{44}\Delta t} \quad e^{-\beta_{55}\Delta t} \quad e^{-\beta_{66}\Delta t} \right]^T, \text{ where } \beta_{ij} \text{ are the decay constants and } \Delta t \text{ is the time}$$

step used in the simulation. \mathbf{B} is the viscoelastic decay matrix given by

$$\mathbf{B} = \begin{bmatrix} \frac{1-e^{-\beta_{11}\Delta t}}{\beta_{11}\Delta t} & \frac{1-e^{-\beta_{12}\Delta t}}{\beta_{12}\Delta t} & \frac{1-e^{-\beta_{13}\Delta t}}{\beta_{13}\Delta t} & 0 & 0 & 0 \\ \frac{1-e^{-\beta_{12}\Delta t}}{\beta_{12}\Delta t} & \frac{1-e^{-\beta_{22}\Delta t}}{\beta_{22}\Delta t} & \frac{1-e^{-\beta_{23}\Delta t}}{\beta_{23}\Delta t} & 0 & 0 & 0 \\ \frac{1-e^{-\beta_{13}\Delta t}}{\beta_{13}\Delta t} & \frac{1-e^{-\beta_{23}\Delta t}}{\beta_{23}\Delta t} & \frac{1-e^{-\beta_{33}\Delta t}}{\beta_{33}\Delta t} & 0 & 0 & 0 \\ 0 & 0 & 0 & \frac{1-e^{-\beta_{44}\Delta t}}{\beta_{44}\Delta t} & 0 & 0 \\ 0 & 0 & 0 & 0 & \frac{1-e^{-\beta_{55}\Delta t}}{\beta_{55}\Delta t} & 0 \\ 0 & 0 & 0 & 0 & 0 & \frac{1-e^{-\beta_{66}\Delta t}}{\beta_{66}\Delta t} \end{bmatrix} \quad (7)$$

The higher the value of the decay constants, the more converging the response of the material would be towards that of the quasi-static response in the elastic regime. This is because as the decay constants increase, the viscous trial stress tends to a zero value. The deformation sub-model uses a plasticity-based formulation with a modified version of Tsai-Wu failure criterion as the yield function as

$$f(\boldsymbol{\sigma}_{TRIAL}) = -1 + (F_1 \ F_2 \ F_3 \ 0 \ 0 \ 0) \boldsymbol{\sigma}_{TRIAL} + \boldsymbol{\sigma}_{TRIAL}^T \mathbf{F} \boldsymbol{\sigma}_{TRIAL} \quad (8)$$

$$\text{where, } \mathbf{F} = \begin{bmatrix} F_{11} & F_{12} & F_{13} & 0 & 0 & 0 \\ F_{12} & F_{22} & F_{23} & 0 & 0 & 0 \\ F_{13} & F_{23} & F_{33} & 0 & 0 & 0 \\ 0 & 0 & 0 & F_{44} & 0 & 0 \\ 0 & 0 & 0 & 0 & F_{55} & 0 \\ 0 & 0 & 0 & 0 & 0 & F_{66} \end{bmatrix}$$

where, F_i 's and F_{ij} 's are the yield function coefficients. In order to check for yielding, the yield function coefficients are computed corresponding to the current yield stress ($\sigma_{ij}^{y,T/C/45}$) using the quasi-static stress-strain input curves as shown in Equation (9), (10), (11) and (12).

$$\begin{aligned} F_1 &= \frac{1}{\sigma_{11}^{y,T}} - \frac{1}{\sigma_{11}^{y,C}} & F_{11} &= \frac{1}{\sigma_{11}^{y,T} \sigma_{11}^{y,C}} & F_{44} &= \frac{1}{(\sigma_{12}^y)^2} \\ F_2 &= \frac{1}{\sigma_{22}^{y,T}} - \frac{1}{\sigma_{22}^{y,C}} & F_{22} &= \frac{1}{\sigma_{22}^{y,T} \sigma_{22}^{y,C}} & F_{55} &= \frac{1}{(\sigma_{23}^y)^2} \\ F_3 &= \frac{1}{\sigma_{33}^{y,T}} - \frac{1}{\sigma_{33}^{y,C}} & F_{33} &= \frac{1}{\sigma_{33}^{y,T} \sigma_{33}^{y,C}} & F_{66} &= \frac{1}{(\sigma_{31}^y)^2} \end{aligned} \quad (9)$$

$$F_{12} = \frac{2}{(\sigma_{12}^{y,45})^2} - \frac{F_1 + F_2}{\sigma_{12}^{y,45}} - \frac{1}{2}(F_{11} + F_{22} + F_{44}) \quad (10)$$

$$F_{23} = \frac{2}{(\sigma_{23}^{y,45})^2} - \frac{F_2 + F_3}{\sigma_{23}^{y,45}} - \frac{1}{2}(F_{22} + F_{33} + F_{55}) \quad (11)$$

$$F_{13} = \frac{2}{(\sigma_{31}^{y,45})^2} - \frac{F_1 + F_3}{\sigma_{31}^{y,45}} - \frac{1}{2}(F_{11} + F_{33} + F_{66}) \quad (12)$$

The plasticity algorithm is used to compute the plastic multiplier ($\Delta\lambda$). The updated stress after the plasticity algorithm is computed using the following equation,

$$\boldsymbol{\sigma} = \left(\boldsymbol{\sigma}_{TRIAL} - [\mathbf{C}_e + (\mathbf{C} - \mathbf{C}_e) \circ \mathbf{B}] \Delta\lambda \frac{\partial h}{\partial \boldsymbol{\sigma}} \Big|_{\boldsymbol{\sigma}_{TRIAL}} \right) \quad (13)$$

h is the plastic potential function given by the following equation,

$$h = \sqrt{H_{11}\sigma_{11}^2 + H_{22}\sigma_{22}^2 + H_{33}\sigma_{33}^2 + 2H_{12}\sigma_{11}\sigma_{22} + 2H_{23}\sigma_{22}\sigma_{33} + 2H_{31}\sigma_{33}\sigma_{11} + H_{44}\sigma_{12}^2 + H_{55}\sigma_{23}^2 + H_{66}\sigma_{31}^2} \quad (14)$$

where H_{ij} are the flow rule coefficients, and the procedure to determine these are presented in Goldberg et al. [2015]. σ_{ij} 's are the stresses in PMDs for the current state of stress. In the previous version of MAT_213 [Hoffarth et al., 2016], at a given point of time during the simulation, the yield stresses were obtained from the input stress-strain curve interpolated for a strain-rate and temperature. These yield stresses are used to compute F_i 's and F_{ij} 's and thereby to compute $\Delta\lambda$. Numerical instabilities are created if there are sudden changes in the strain rate that is typical in impact analyses. In the new modified approach, the interpolation of the yield stresses are done using the effective plastic strain rate. In order to carry out this new interpolation scheme, each stress-strain curve needs to be assigned an effective plastic strain rate. For a given input stress-strain curve, an increment of effective plastic strain ($\Delta\lambda$) is computed for every increment of strain ($\Delta\varepsilon$), during the preprocessing step in MAT_213. The number of increments (n) depends on the user. The strain rate designated for each stress-strain curve by the user is converted into an equivalent effective plastic strain rate by MAT_213 using the following equation,

$$\dot{\lambda} = f_{mean} \dot{\varepsilon} \quad (15)$$

where

$$f_{mean} = \frac{\sum_1^n \frac{\Delta\lambda}{\Delta\varepsilon}}{n}$$

The effective plastic strain rate changes gradually even if there is a sudden change in the strain rate. This new approach also takes care of a stress relaxation problem. This is explained with an example in the verification test section. The equilibrium and the viscous stresses need to be updated to be used in the next time step for the computation of trial stresses. It should be noted that the summation of the updated equilibrium and the viscous stresses are equal to the updated stress shown in Equation (13).

The viscous and the equilibrium stresses are updated depending on the yield function value computed based on the equilibrium trial stresses, $f(\sigma_{TRIAL}^e)$, using the Equations (16) and (17). This is based on $f(\sigma_{TRIAL}^e)$ so that the stresses do not drop below the quasi-static yield stress in case of a stress relaxation.

$$f(\sigma_{TRIAL}^e) \leq 0, \sigma^v = \sigma_{TRIAL}^v - [C \circ B] \Delta\lambda \left. \frac{\partial h}{\partial \sigma} \right|_{\sigma_{TRIAL}} \tag{16}$$

$$f(\sigma_{TRIAL}^e) > 0, \sigma^e = \left(\sigma_{TRIAL}^e - C_e \Delta\lambda \left. \frac{\partial h}{\partial \sigma} \right|_{\sigma_{TRIAL}} \right) \text{ and } \sigma^v = \sigma_{TRIAL}^v - [(C - C_e) \circ B] \Delta\lambda \left. \frac{\partial h}{\partial \sigma} \right|_{\sigma_{TRIAL}} \tag{17}$$

Verification Tests

The verification of MAT_213 with the enhanced features was done with T800/F300 unidirectional composite [Toray, 2020]. The stress-strain curves obtained from experiments [Khaled et al., 2017] were used to drive MAT_213 deformation sub-model (damage and failure sub-models were de-activated). For illustration of the strain-rate smoothing feature, a single element 1-direction tension test model is considered. Eight-noded hexahedron element is used to model this test (Figure 1). The PMDs are marked within the cube with the fiber direction represented by the green color line. The dashed red color arrows represent a restraint along the direction of the arrow. All the translational displacements are restrained at the pin support. The black color arrows represent a prescribed displacement to induce a strain-rate of 1/s.

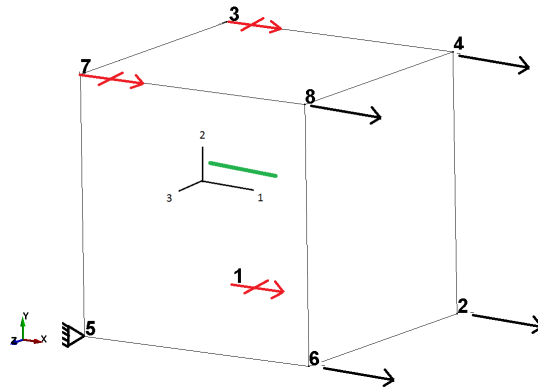


Figure 1. 1-direction tension schematic

The strain-rate obtained in the normal component from the simulation for different values of *FILT* are shown in Figure 2. In each of the graphs, “T1”, “C2” and “C3” represents the strain-rate in the 1-direction tension, 2-direction compression and 3-direction compression components, respectively. As can be seen, the oscillations in the strain-rate in the 2 and the 3-direction compression components decreases as the value of *FILT* increases.

Figure 3 shows the schematic of the finite element (FE) model of the single element 2-direction compression test. A constant strain rate of approximately 1300/s is induced due to the applied displacement till the strain in the element in the 2-direction reaches a value of ~0.04. Thereafter, the strain was held constant at a value of ~0.04 in compression as shown in Figure 4(a).

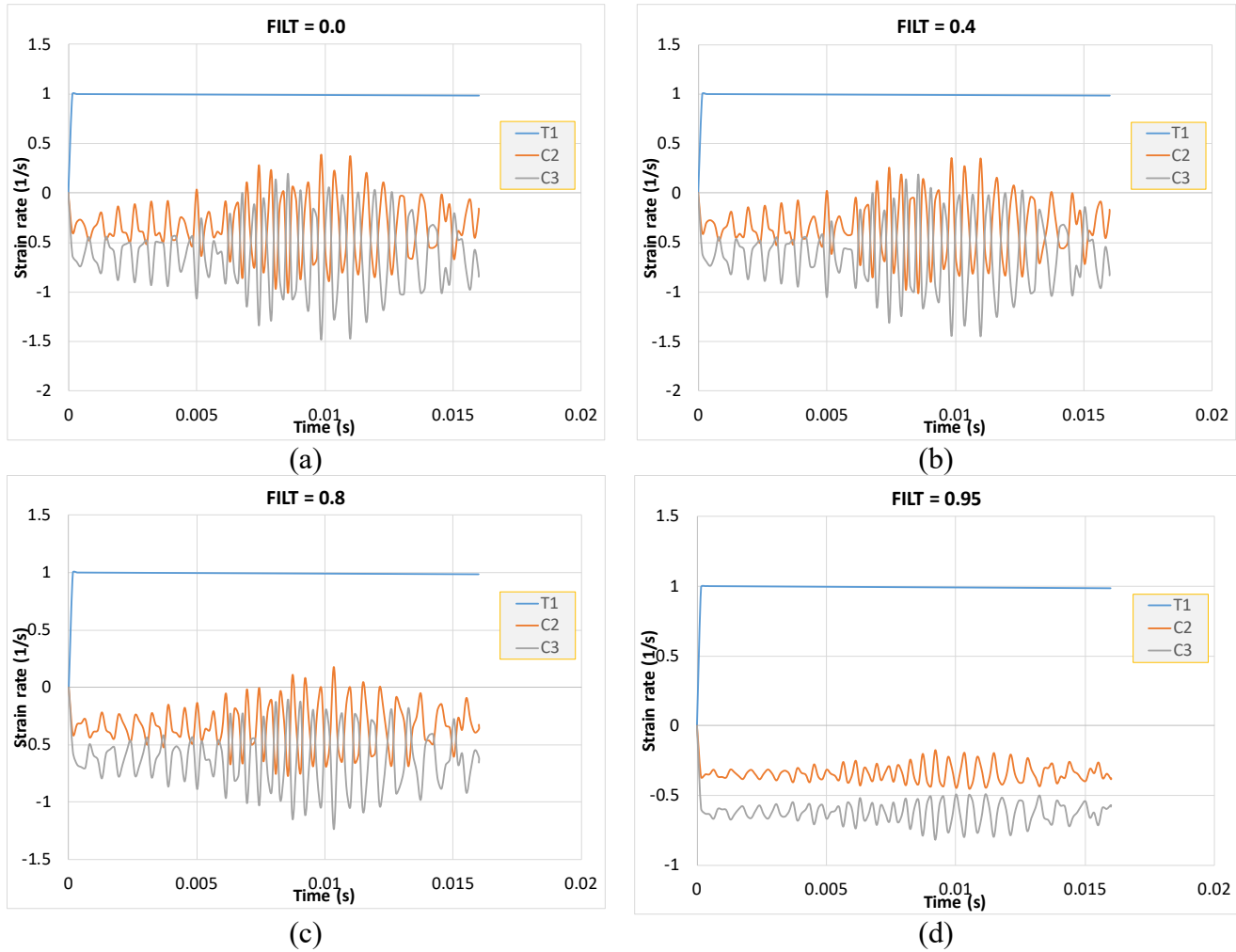


Figure 2. 1-direction tension test strain-rates in the three normal components for (a) $FILT = 0$ (b) $FILT = 0.4$ (c) $FILT = 0.8$ (d) $FILT = 0.95$

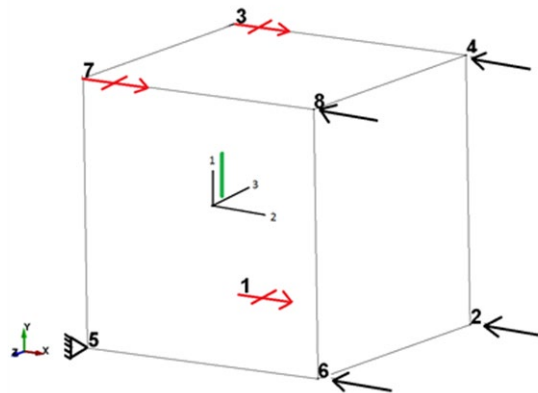


Figure 3. 2-direction compression schematic

The stress obtained from MAT_213 simulation is shown in Figure 4(b). The corresponding stress-strain response and the rates are shown in Figure 4(c) and (d), respectively. For the 2-direction component, there are two input stress-strain curves as shown in Figure 4(c). “Model (QS-RT)” and “Model (1300/s)” represent the input given into MAT_213 with a designated strain rate of 0.0001/s and 1300/s, respectively. The stress-strain data used for “Model (QS-RT)” is obtained from quasi-static room temperature (QS-RT) testing [Khaled et al., 2017]. The stress-strain data used for “Model (1300/s)” is obtained from high rate testing done by our research collaborators at Ohio State University. “MAT_213 (1300/s)” represents the stress-strain response obtained from simulation using MAT_213.

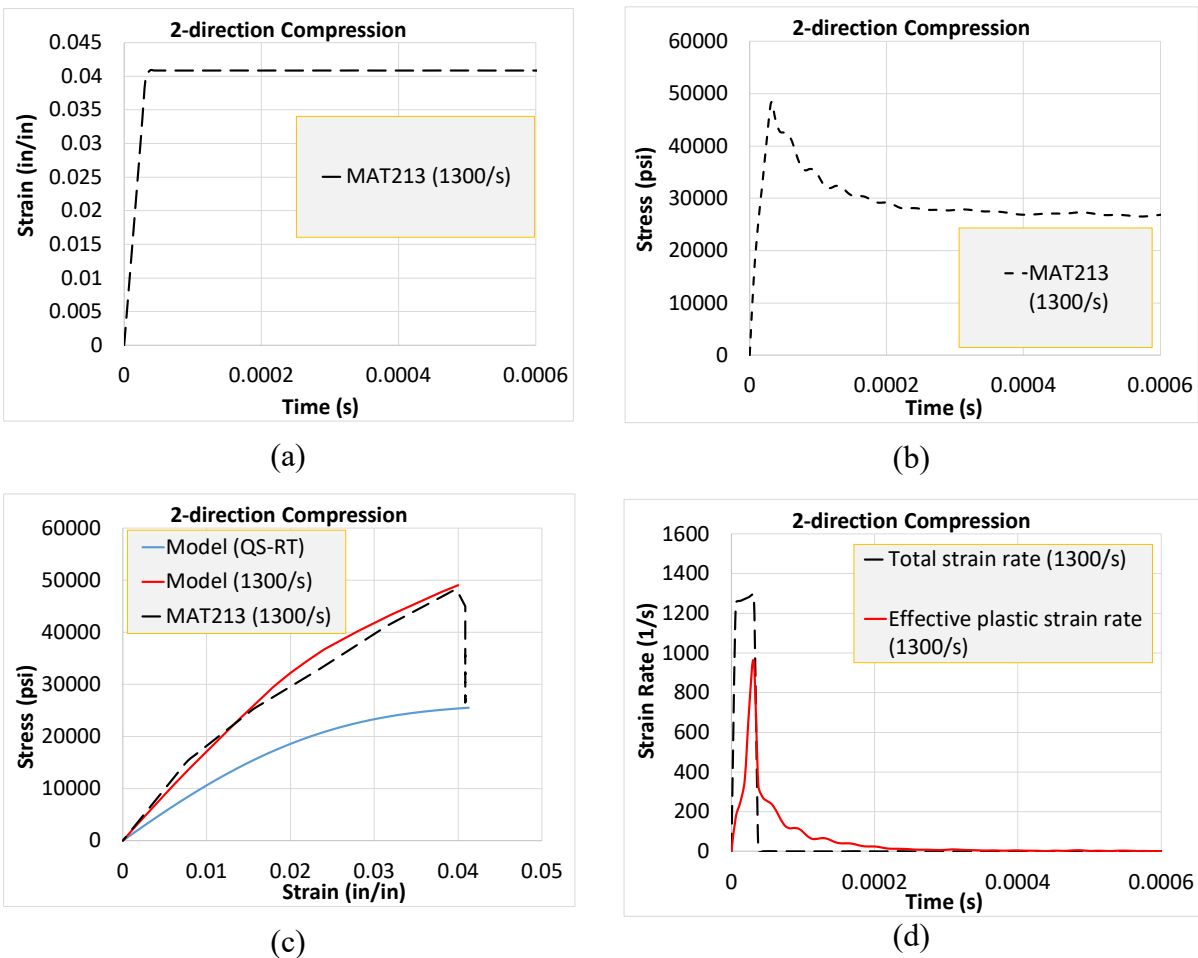
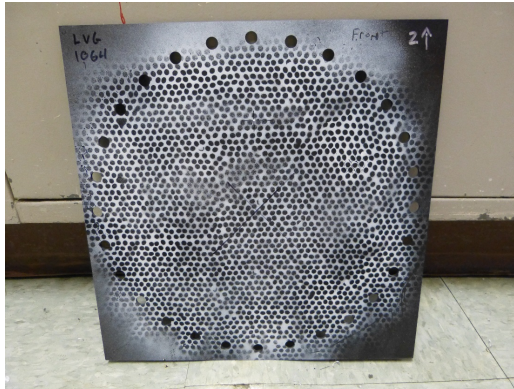


Figure 4. 2-direction compression test results (a) Strain-time history (b) Stress-time history (c) Stress-strain curve (d) Rate-time history

It can be observed that the stress gradually reduces to the “peak stress of the QS-RT curve” and stays constant after the strain is held constant. This is because the effective plastic strain rate gradually goes to zero, and so the interpolated flow stress used for the plasticity computation corresponds to the input stress-strain curve with the lowest effective plastic strain rate (QS-RT curve in this case). Previous implementation would yield a sudden drop in the stress value since the interpolation of the stresses were done using the total strain rate rather than the effective plastic strain rate [Hoffarth et al., 2016].

Validation Test

A ballistic plate impact test was considered for validating MAT_213. This involves a composite panel made of T800/F3900 composite with the lay-up, $[(0/90/45/-45)_2]_S$ subjected to an aluminum projectile at a velocity of 236 ft/s. The experiment was conducted at NASA-Glenn Research Center (NASA-GRC). The composite panel has a dimension of 12 x 12 x 0.122 inches as shown in Figure 5(a). The projectile weighs 50 g as shown in Figure 5(b). The projectile is fired using a gas gun. The response of the plate is recorded using Digital Image Correlation (DIC) technique.



(a)



(b)

Figure 5. (a) Composite panel before the test (b) Aluminum projectile

The panel is modeled using 16 elements through the thickness to model each of the 16 plies. Between each of these plies in the model, there are cohesive zone elements. This is done to predict the delamination behavior. The plies are modeled using MAT_213, whereas the cohesive zone elements are modeled using MAT138 [Khaled et al., 2018]. *CONTACT_ERODING_SURFACE_TO_SURFACE contact definition is used to model the interaction between the projectile and the plate. *CONTACT_ERODING_SINGLE_SURFACE contact definition is used to model the interaction between each ply. The aluminum projectile is modeled using *MAT_PIECEWISE_LINEAR_PLASTICITY [Shyamsunder et al., 2018]. The FE model is shown in Figure 6 with the boundary conditions. Figure 6(a) shows the marked nodes which are restrained in the in-plane displacements to mimic bolts used in the experiment. Figure 6(b) shows the marked nodes restrained in the out-of-plane displacement to mimic the clamping done during the experiment. Figure 6 also shows the projectile just before the impact which is given an initial velocity.

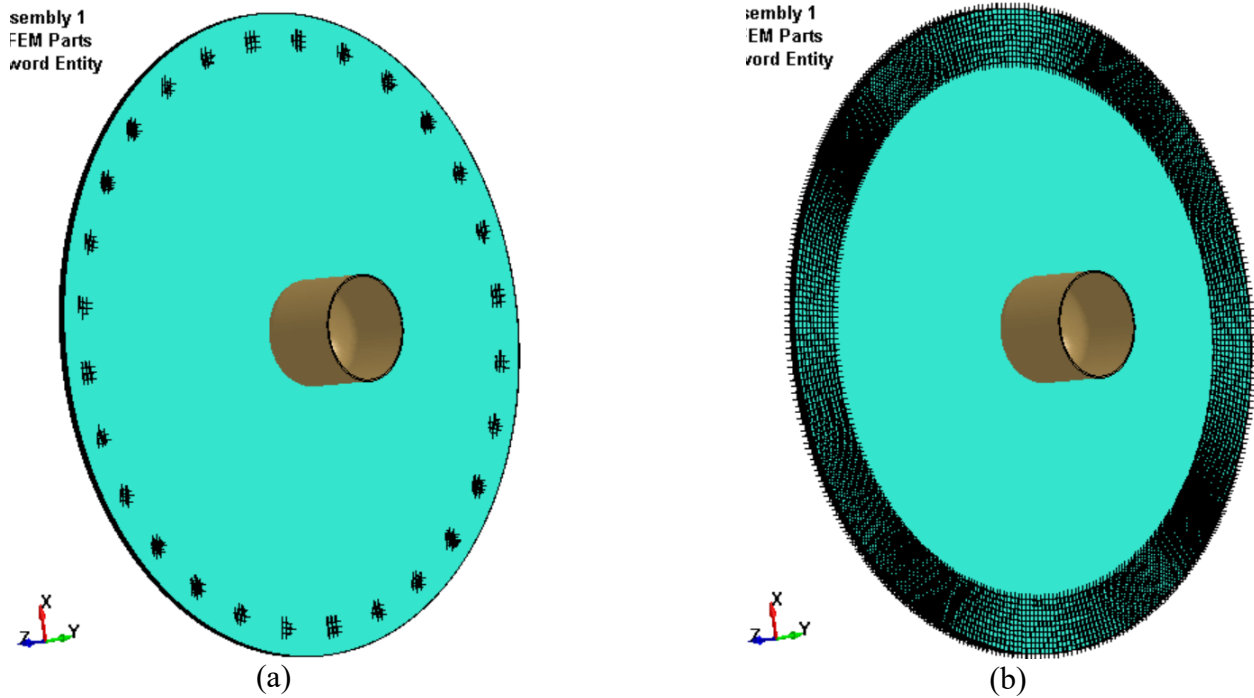


Figure 6. LS-DYNA finite element model (a) nodes restrained in in-plane displacement, (b) nodes restrained in out-of-plane displacement

In order to compare the experimental and the simulation results, the out-of-plane displacement on the back side of the plate was chosen as the metric. Figure 7 shows the out-of-plane displacement plotted against time. Two different simulations were run using MAT_213. “MAT_213- With Rate Data” was run using rate dependent stress-strain curves in addition to the QS-RT. These additional curves were the 2-direction compression curve with the legend “Model (1300/s)” in Figure 4(c) and 2-direction tension curve at a strain rate of 325/s as shown in Figure 7(a). “MAT13- Without Rate Data” was run only using the QS-RT stress-strain curves [Khaled et al., 2017].

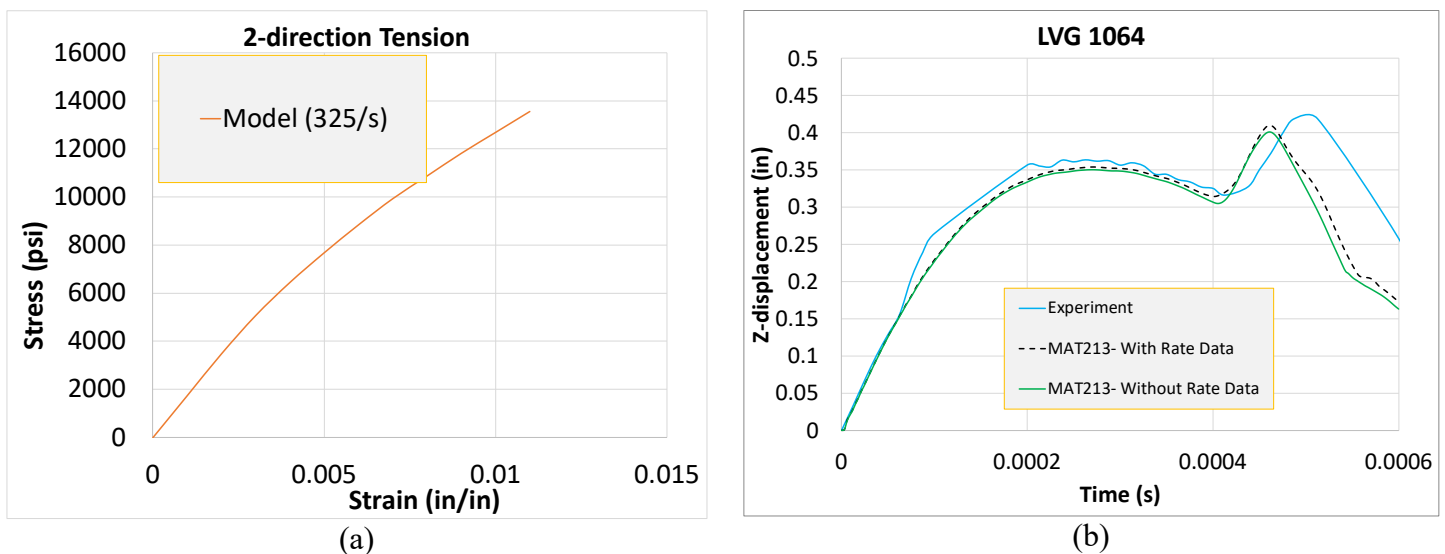


Figure 7. (a) High rate stress-strain data in the 2-direction tension (b) Comparison of out-of-plane displacement on the back face of the panel

Both the MAT_213 simulation responses slightly under predict the peak displacement as shown in Figure 7(b). Investigation is underway, to consider the rate dependent stress-strain in the 3-direction as well by assuming transverse isotropy. The authors believe that this can improve the prediction since the impact load is applied in the out-of-plane direction. While there are small differences in the response obtained from simulations run with and without the rate data, the difference would be more significant if the simulation is run for a longer duration since then the relaxation taking place in case of “with rate data” will be more pronounced. In our present study, the simulation was carried out for 0.0006 s with the primary objective to compare the peak displacement. Figure 8 shows the comparison of the delamination pattern of the plate. Figure 8(a) shows the ultra-sonic scan of the composite panel obtained after the experiment at NASA-GRC. The FE model was made 100% transparent and the deleted elements were highlighted to get the delamination pattern (only the cohesive zone elements get deleted). The delamination pattern obtained from the simulation run without the rate data and with the rate data are shown in Figure 8(b) and (c), respectively. The circle in the figures is the outline of the FE model, and dark portion in the middle is the delaminated zone. Both the simulation results are in good agreement with the experimentally obtained image.

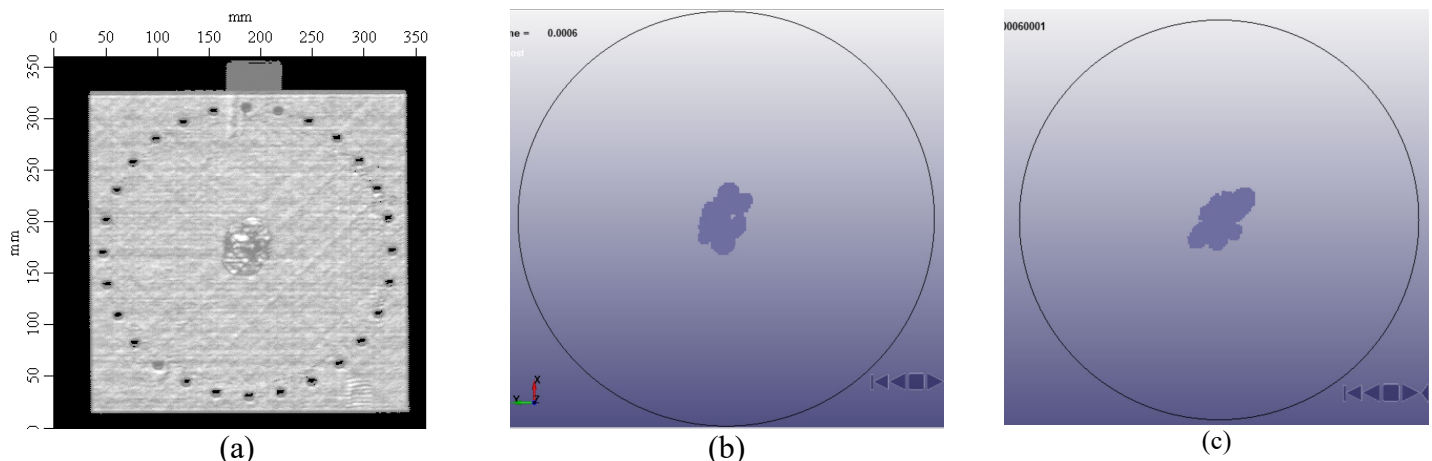


Figure 8. (a) UT-scan after the testing (b) Delamination pattern from “MAT_213 – Without rate data” (c) Delamination pattern from “MAT_213 – With rate data”

Conclusions

The implementation of the new features in MAT_213 deformation sub-model has been discussed. Single element tests used for the verification are presented. The strain smoothing technique and the stress relaxation response with the incorporation of rate-dependent stress-strain data are shown using these examples. A ballistic impact test was used to validate the aforementioned implementation scheme. It has been shown that the response is accurately predicted.

Acknowledgements

Authors Shyamsunder, Khaled, and Rajan gratefully acknowledge the support of (a) the Federal Aviation Administration through Grant #12-G-001 titled “Composite Material Model for Impact Analysis”, William Emmerling and Dan Cordasco, Technical Monitors, and (b) NASA through Contract Number: NN15CA32C titled “Development and Implementation of an Orthotropic Plasticity Progressive Damage Model for Transient Dynamic/Impact Finite Element Analysis of Composite Structures”, Robert Goldberg, Contracting Officer Representative.

References

- Achstetter, Tobias. (2019). "Development of a Composite Material Shell-Element Model for Impact Applications", PhD Dissertation, George Mason University, Fairfax, VA, USA.
- Goldberg, R., Carney, K., DuBois, P., Hoffarth, C., Harrington, J., Rajan, S.D. and Blankenhorn, G. (2015). "Development of an Orthotropic Elasto-Plastic Generalized Composite Material Model Suitable for Impact Problems", ASCE J of Aerospace Engineering, DOI: 10.1061/(ASCE)AS.1943-5525.0000580.
- Goldberg, R., Carney, K., DuBois, P., Hoffarth, C., Khaled, B., Shyamsunder, L., Rajan, S.D. and Blankenhorn, G. (2017). "Implementation of a Tabulated Failure Model Into a Generalized Composite Material Model Suitable for Use in Impact problems", American Society for Composites, Thirty-Second Technical Conference, 2017, Purdue University, West Lafayette, Indiana, USA.
- Hoffarth, C., Rajan, S.D., Goldberg, R., Carney, K., DuBois, P. and Blankenhorn, G. (2016). Implementation and Validation of a Three-Dimensional Material Model for Orthotropic Composites, Composites Part A: Applied Science and Manufacturing, 91(1), 336-350.
- Khaled, B., Shyamsunder, L., Hoffarth, C., Rajan, S.D, Goldberg, R., Carney, K., DuBois, P., and Blankenhorn, G. (2017). "Experimental Characterization of Composites to Support an Orthotropic Plasticity Material Model", J of Composite Materials, DOI: 10.1177/0021998317733319, August 2017.
- Khaled, B., Shyamsunder, L., Hoffarth, C., Rajan, S.D, Goldberg, R., Carney, K., DuBois, P., and Blankenhorn, G. (2018). "Damage Characterization of Composites to Support an Orthotropic Plasticity Model", J of Composite Materials, 53(7), 941–967.
- Lempriere, B.M. (1968). "Poisson's Ratio in Orthotropic Materials", American institute of Aeronautics and Astronautics journal, 6(11), 2226-2227.
- LSTC (2019). LS-DYNA R11, <http://lstc.com/products/ls-dyna>
- Shyamsunder, L., Khaled, B., Hoffarth, C., Rajan, S. D., Goldberg, R. K., Carney, K. S., DuBois, P., and Blankenhorn, G. (2018). "Using MAT_213 for Simulation of High-Speed Impacts of Composite Structures", 15th International LS-DYNA User's Conference, Dearborn, USA.
- Shyamsunder, L., Khaled, B., Rajan, S. D., Goldberg, R. K., Carney, K. S., DuBois, P., and Blankenhorn, G. (2019). "Implementing deformation, damage and failure in an orthotropic plastic material model." J of Composite Materials, DOI: 10.1177/0021998319865006, July 2019.
- Toray Carbon Fibers America. <https://www.toraycma.com/> (2020, last accessed Mar 23, 2020).